European Journal of Medicinal Chemistry 178 (2019) 81–92

Contents lists available at ScienceDirect

European Journal of Medicinal Chemistry

journal homepage: http://www.elsevier.com/locate/ejmech

Research paper

Synthesis and biological evaluation of 5-aminoethyl benzophenanthridone derivatives as DNA topoisomerase IB inhibitors

Wen-Lin Tang [a, b], Yu Zhang [a], De-Xuan Hu [a], Hui Yang [a], Qian Yu [a], Jian-Wen Chen [a], Keli Agama [c], Yves Pommier [c], Lin-Kun An [a, b, *]

[a] School of Pharmaceutical Sciences, Sun Yat-sen University, Guangzhou, 510006, China
[b] Guangdong Provincial Key Laboratory of New Drug Design and Evaluation, Guangzhou, 510006, China
[c] Developmental Therapeutics Branch, Center for Cancer Research, National Cancer Institute, National Institutes of Health, Bethesda, MD, 20892, USA

ARTICLE INFO

Article history:
Received 29 March 2019
Received in revised form
27 May 2019
Accepted 27 May 2019
Available online 30 May 2019

through a transesterification reaction by nucleophilic attack of its catalytic tyrosine (Tyr723 for human TOP1) to the DNA phosphodiester backbone to form the enzyme-DNA covalent cleavage complexes (TOP1cc). TOP1cc are transient intermediates under normal physiological circumstances as they reverse into the intact DNA and release TOP1 [4,5]. TOP1 inhibitor, such as camptothecin (CPT, Fig. 1) can bind at the interface of TOP1cc [6–8], which stabilizes TOP1cc and prevents further religation of the nicked DNA, resulting in DNA damage and triggering cell death [4,5]. Therefore, TOP1 is a validated target for the discovery of anticancer agents [4,6,9,10].

To date, four well-known camptothecin derivatives (Fig. 1) have been approved for clinical treatment of cancers, including Topotecan and Irinotecan approved by FDA [11–13], 10-hydroxycamptothecin (HCPT, in China) and Belotecan (in South Korea) [4,14–16]. In spite of their effectiveness in solid tumors, camptothecin TOP1 inhibitors suffer from many shortcomings, such as chemical instability under physiological condition, poor solubility, bone marrow dose-limiting toxicity, severe gastrointestinal toxicity for Irinotecan and drug efflux-mediated resistance [9,17]. Therefore, many investigations have focused on the discovery of non-camptothecin TOP1 inhibitors. And three chemotypes of non-camptothecin TOP1 inhibitors, including indolocarbazole, dibenzonaphthyridinone and indenoisoquinoline derivatives, have been developed [9,18,19]. Three indenoisoquinolines LMP400L, MP744 and LMP776 (Fig. 1) are in clinical trials [19].

Natural products are important sources for medicinal chemistry and drug development. To find novel non-camptothecin TOP1 inhibitors, we studied our in-house natural product library and found several chemotypes inhibiting TOP1, including oxynitidine and meroterpenoid derivatives. Further investigation indicated that several meroterpenoid derivatives showed high TOP1 relaxing inhibition, but were not able to trap and stabilize TOP1cc and could be classified as TOP1 catalytic inhibitors [20, 21]. On the contrary,

* Corresponding author. School of Pharmaceutical Sciences, Sun Yat-sen University, Guangzhou, 510006, China. Tel. and
E-mail address: lssalk@mail.sysu.edu.cn (L.-K. An).

https://doi.org/10.1016/j.ejmech.2019.05.074

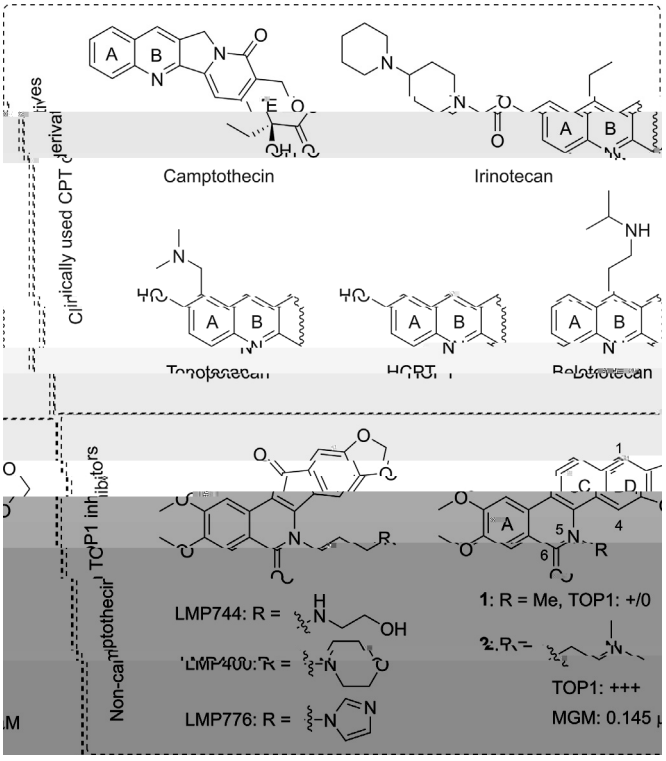

Fig. 1. Structures of the camptothecins in clinical uses, indenoisoquinolines in clinical trials and the oxynitidine TOP1 inhibitors found in our laboratory.

oxynitidine (**1**, Fig. 1) exhibited weak TOP1 cleavage inhibitory activity (+/0) [22]. Structural optimization of **1** gave several TOP1 inhibitors with higher inhibitory activity, including NTD-96 (**2**, Fig. 1). **2** shows increased TOP1 inhibition (+++) and traps TOP1cc at genome binding sites different from CPT [22]. Further investigation indicated that **2** targets to TOP1 in cells, inducing cellular TOP1cc formation and DNA damage, and exhibits good antitumor activity both *in vitro* and *in vivo* [22]. Structure-activity relationship (SAR) analysis indicated that [22]: 1) the carbonyl group at the 6-position (benzophenanthridinone derivatives) is important for TOP1 inhibition. Most of the 6-aminoalkyloxy benzophenanthridine derivatives have no TOP1 inhibition at 100 μM concentration and show weak cytotoxicity. Furthermore, the reduced derivatives (dihydrobenzophenanthridine) show weak both TOP1 inhibition and cytotoxicity; 2) substitution of aminoethyl group at the 5-position may increase both TOP1 inhibition and cytotoxicity. It is noteworthy that bigger substituents at the 5-position, for example aminopropyl group did not significantly increase the potency of the drugs as TOP1 inhibitors. To further study the spatial effect of the terminus of the aminoethyl group at 5-position on the TOP1 inhibition, in this work, a series of novel 5-aminoethyl substituted benzophenanthridinone derivatives was synthesized and biologically evaluated.

2. Results and discussion

2.1. Chemistry

The synthesis of the designed 5-aminoethyl substituted benzophenanthridinone derivatives is outlined in Scheme 1. Similar to our previous publication [22], the hydroxy group of the Schiff base **3** prepared from the reaction of 6-bromoveratraldehyde with 2-aminoethanol was protected using methoxymethyl (MOM) group to give the intermediate **4**, which was directly used for the next reaction without further purification. The intermediate **6** was obtained in two steps. First, under nickel-based catalysis [23], the cyclization reaction of **4** with **5**, prepared through Sonogashira coupling reaction according to the reported method [24], gave a ternary ammonium salt intermediate. In the second step, the resulting ternary ammonium salt intermediate was oxidized by $K_3Fe(CN)_6$ to give the intermediate **6**. Following the Swern oxidation of the hydroxy group of **6**, the cyclization reaction under concentrated hydrochloric acid condition gave the intermediate **8** with simultaneous deprotection of MOM group. The replacement of hydroxy group of **8** with bromine gave the bromide **9** in 91% yield. Following replacement reaction of **9** with NaN_3, the Pd/C catalytic reduction reaction under hydrogen atmosphere gave the target amine **11** in 51% yield for the two steps (from **9**). **11** reacted with formaldehyde to form a Schiff base, which could be reduced by zinc powder to give the target product **12** in 59% yield. The acylation reaction of **12** with various acyl chloride in dichloromethane gave the target products **13**–**19** with *N*-methyl amide group as the terminus of the side chain at the 5-position. Similarly, the acylation of **11** gave the target products **20**–**25**. Finally, we synthesized fifteen benzophenanthridone derivatives with various termini groups of the aminoethyl side chain at the 5-position, including amino group, methylamino group, amide group, sulfonamide group and phosphoamide group. Their structures and purity were assessed through HRMS, 1D and 2D NMR spectra, and HPLC method.

2.2. TOP1 inhibition

The synthesized compounds were tested for TOP1 inhibitory activity through TOP1-mediated cleavage assay using a 3′-[^{32}P]-labeled double-stranded DNA fragment as substrate along with CPT and LMP744, an indenoisoquinoline TOP1 inhibitor [25], as positive controls [26]. All compounds were tested at four concentrations, 0.1, 1.0, 10 and 100 μM. The TOP1-mediated cleavage activity of the compounds was semiquantitatively graded consistent with prior publications based on the number and intensities of the DNA cleavage bands relative to the TOP1 inhibition of CPT at 1 μM concentration [22,25]: 0, no inhibitory activity; +, between 20% and 50% inhibitory activity; ++, between 50% and 75% inhibitory activity; +++, between 75% and 95% inhibitory activity; ++++, equal inhibitory activity to CPT. The TOP1-mediated cleavage activity of the synthesized compounds is summarized in Table 1. Compared to the parent **1**, most of the synthesized compounds showed increased TOP1 inhibitory activity except for three compounds **13**, **22** and **24**, which showed equal activity to **1**. Compound **12** showed the most potent TOP1 inhibition of +++, equal to compound **2** [22]. Five compounds **11**, **18**, **19**, **20** and **23** showed moderate TOP1 inhibitory activity (++). Compared with **2**, the bigger termini of the side chain seem to decrease of TOP1 inhibitory activity. Representative TOP1-mediated cleavage assay gel is shown in Fig. 2. Compounds **11**, **12**, **18**–**20** and **23** exhibited the ability to induce TOP1-mediated cleavage bands in a dose-dependent manner with cleavage sites similar to LMP744 but not to CPT. For example, the cleavage sites 17, 35 and 79 could be induced by **11**, **12**, **18**–**20** and **23** but not by CPT, implying that the synthesized benzophenanthridinone derivatives trap TOP1cc at different DNA sequence from CPT.

To inspect the molecular binding mode of the synthesized TOP1 inhibitors within the TOP1-DNA complex, molecular modeling was performed. A hypothetical binding model was built using in-silico docking from the X-ray crystal of the TOP1-DNA-ligand ternary complex (PDB ID: 1K4T) [7]. Compounds were energy-minimized and docked into the binding model. As shown in Fig. 3A, the benzophenanthridinone scaffold of **12** intercalates in the DNA break

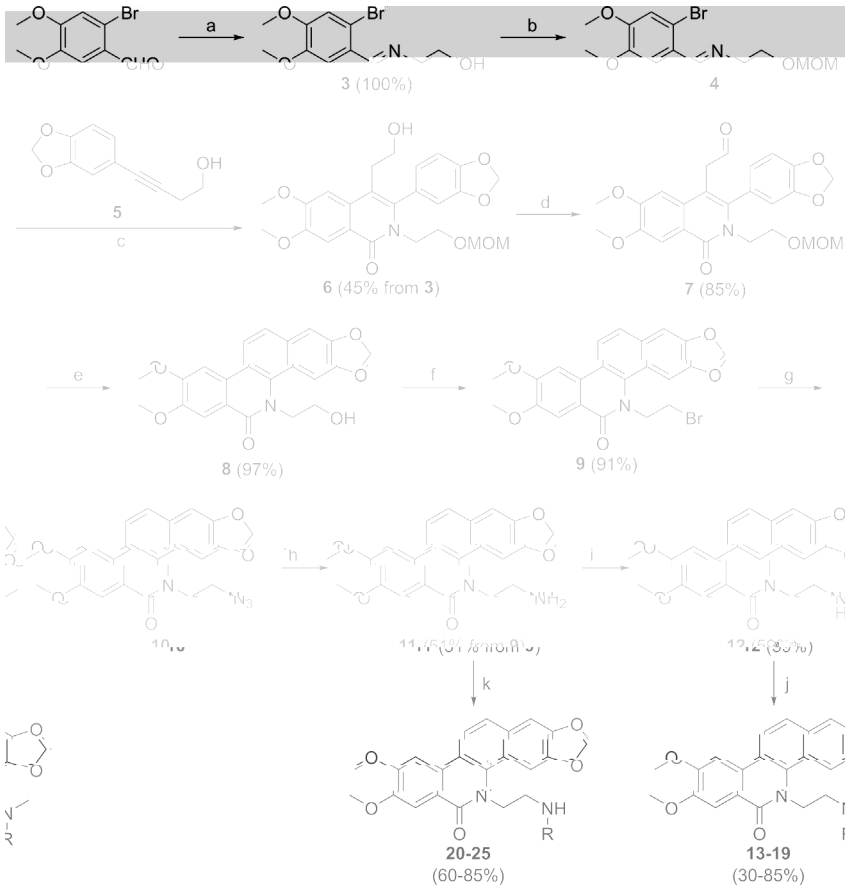

Scheme 1. The synthesis of the target compounds
Reagents and conditions: (a) MeOH, $NH_2(CH_2)_2OH$, rt. (b) MOMCl, NaH, THF, 0 °C. (c) I) N_2, $Ni(cod)_2$, P(*o*-Tol)$_3$, MeCN, 80 °C; ii) CsOH, $K_3[Fe(CN)_6]$, MeOH, H_2O, 80 °C. (d) $(COCl)_2$, DMSO, TEA, DCM, −60 °C. (e) concd. hydrochloric acid, MeOH, rt. (f) PBr_3, TCM, rt. g) NaN_3, DMSO, rt. (h) Pd/C, H_2, THF, rt. (i) aqueous HCHO, Zn, CH_3CO_2H, H_2O, rt. (j) Acyl chloride, DIPEA, DCM, reflux. (k) Acyl chloride, DIPEA, DCM, rt.

made by TOP1 and readily stacks with the +1 and −1 base pairs flanking the DNA cleavage site, similar to that of **2** [22]. The A- and B-ring of **12** stack with the bases of non-cleaved strand (C and A), while the C- and D-ring stack with the scissile strand bases (G and T). In addition, the methylaminoethyl side chain of **12** extends into the minor groove of the DNA and binds to a limited space (Fig. 3B), which might be the reason why the bigger termini of the side chain decrease TOP1 inhibitory activity. Also, a hydrogen bond (2.9 Å) was observed between the lactam oxygen atom and R364 residue (Fig. 3A), implying the importance of hydrogen bond acceptor, which is consistent with the cytotoxicity of **12** against the prostate cancer cells DU145-RC0.1, resistant cells with a R364H mutation of TOP1 [27]. DU145-RC0.1 cells showed high resistance to **12** (Table 3). In addition, a hydrogen bond observed between the oxygen atom in the dioxole ring and Asn722 (3.5 Å) might also contribute to the TOP1cc inhibition.

2.3. Cytotoxicity

The cytotoxicity of the synthesized benzophenanthridone derivatives was evaluated through MTT assay against four human tumor cell lines: colon cancer HCT116, breast cancer MCF-7, prostate cancer DU-145 and non-small cell lung cancer A549 cell lines. The compounds were incubated with cells for 72 h in a five-dose assay ranging from 0.01 to 100 μM concentration. At the end of the incubation, MTT solution was added to test the percentage growth of tumor cells. The GI_{50} values, defined as the concentrations of the compounds that resulted in 50% cell growth inhibition, are calculated and summarized in Table 1.

With the increased TOP1 inhibitory activity (+, ++ and +++), the novel synthesized benzophenanthridone analogues **11**, **12**, **14**–**21**, **23** and **25** exhibited increased cytotoxicity against these four tumor cell lines compared with the parent **1** with TOP1 inhibition of +/0, except for **17**, which exhibited decreased cytotoxicity against MCF-7 cells. **12** with the most potent TOP1 inhibition of +++ showed the highest cytotoxicity against HCT116 (GI_{50} = 0.036 μM), MCF-7 (GI_{50} = 0.090 μM), DU145 (GI_{50} = 0.002 μM) and A549 (GI_{50} = 0.97 μM) cell lines. Although **12** has the similar structure and equal TOP1 inhibition to **2**, it showed higher cytotoxicity against HCT116, MCF-7 and DU145 cells, which might possibly due to its good solubility and cellular permeability. Indeed, **12** has higher bioavailability (20.4%, Table 4) *in vivo* than **2** (15.5%) [22]. Furthermore, **12** showed highest cytotoxicity against DU145 cells at low nanomolar concentration (0.002 μM). With the bigger steric terminus of the side chain at the 5-position, the acylated analogues **13**–**25** showed decreased both TOP1 inhibitory activity and cytotoxicity compared **12**, which is consistent with molecular modelling analysis.

Compounds **11** and **12** were submitted to the National Cancer Institute (NCI, USA) for further study on cytotoxicity against the 60 cancer cell lines representation nine tissue types (NCI-60) [28–30]. According to the NCI established procedures, the cells were incubated with **11** or **12** for 48 h and stained with sulforhodamine B dye. The GI_{50} values were plotted and summarized in Table 2. The

results indicate that **12** has a higher mean graph midpoint (MGM) for growth inhibition of all cancer cell lines of 0.0977 μM than that of **11** (0.525 μM) and **2** (0.145 μM) [22]. **12** shows high cytotoxicity against 28 cancer cell lines at nanomolar range (<100 nM) and the most cytotoxic against leukemia SR with GI_{50} of 0.0173 μM.

The cytotoxicity of **12** was further assessed against a panel of isogenic CPT- and doxorubicin-resistant cell lines through MTT assay. The HCT116-siTOP1 subline was established by transfection

close to the catalytic tyrosine and can stabilize the open form of TOP1cc [7,8]. Compared to the parental DU145 cells, the DU145-RC0.1 cells show 225-fold resistant to CPT and 215-fold resistant to **12** (Table 3), which is consistent with the molecular modeling result (Fig. 3) showing a hydrogen bond between **12** and R364 residue. P-Glycoprotein (P-gp) mediated drug efflux is generally responsible for classical multiple drug resistance [33]. The chemotherapeutic agent doxorubincin (DOX) is a substrate of P-gp. Compared to the parental MCF-7 cells, the breast cancer MCF-7/ADR cells overexpressing P-gp are highly resistant to DOX (77.8-fold) and less resistant to **12** (13.7-fold, Table 3) [34], implying **12** might not be a substrate of P-gp. These results indicate that **12** acts as TOP1 inhibitor in cancer cells, similar to its analogue **2** [22].

2.4. Induction of cellular TOP1cc and DNA damage

To assess the induction of TOP1cc by **12**, the immunocomplex of enzyme to DNA (ICE) assay in HCT116 cells was performed. As shown Fig. 4A, both the positive control CPT and **12** induce the formation of cellular TOP1cc in a dose-dependent manner. And **12** shows higher ability to induce cellular TOP1cc at 25 μM than CPT.

To evaluate the DNA damaging effect of **12** in cancer cells, γH2AX foci were assessed by immunofluorescence microscopy in human prostate cancer HCT116 cells. After incubation with drugs for 3 h, HCT116 cells were stained with γH2AX antigt1134.5(bTJ0-200.

into two groups (n = 2) and treated by intravenous injection (iv) at 1 mg/kg dose and intragastrical administration (ig) at 5 mg/kg dose, respectively. Plasma samples were collected postdosing and the concentration of **12** was measured. The PK parameters were calculated and summarized in Table 4. After iv treatment, the $AUC_{0\rightarrow t}$ is 47.2 ± 1.8 h ng/ml and $T_{1/2}$ is 1.21 ± 0.14 h. After ig treatment, T_{max} is 2 ± 0 h and C_{max} is 19 ± 9 ng/ml. The bioavailability (F, 20.4%) of **12** is higher than that of the analogue **2** (15.5%), which might be the reason why **12** shows higher cytotoxicity *in vitro* and antitumor efficiency *in vivo* (Fig. 7) [22].

2.7. Acute toxicity in vivo

The acute toxicity of **12** was assessed in Kunming male mice. The mice were randomly divided into six groups (n = 6) and treated with **12** by intraperitoneal injection (ip) at single doses of 300, 240, 192, 153.6 and 122.9 mg/kg. The control group was treated with sterile water. As shown in Fig. 6, after 7 days of administration with **12**, all mice survived in the group of 122.9 mg/kg dose, and four mice survived in the 153.6 mg/kg dose group, three mice survived in the 192 mg/kg dose group, two mice survived in the 240 mg/kg dose group. All mice died within 5 days in the 300 mg/kg dose group. The median lethal dose (LD_{50}), defined as the dose to kill half

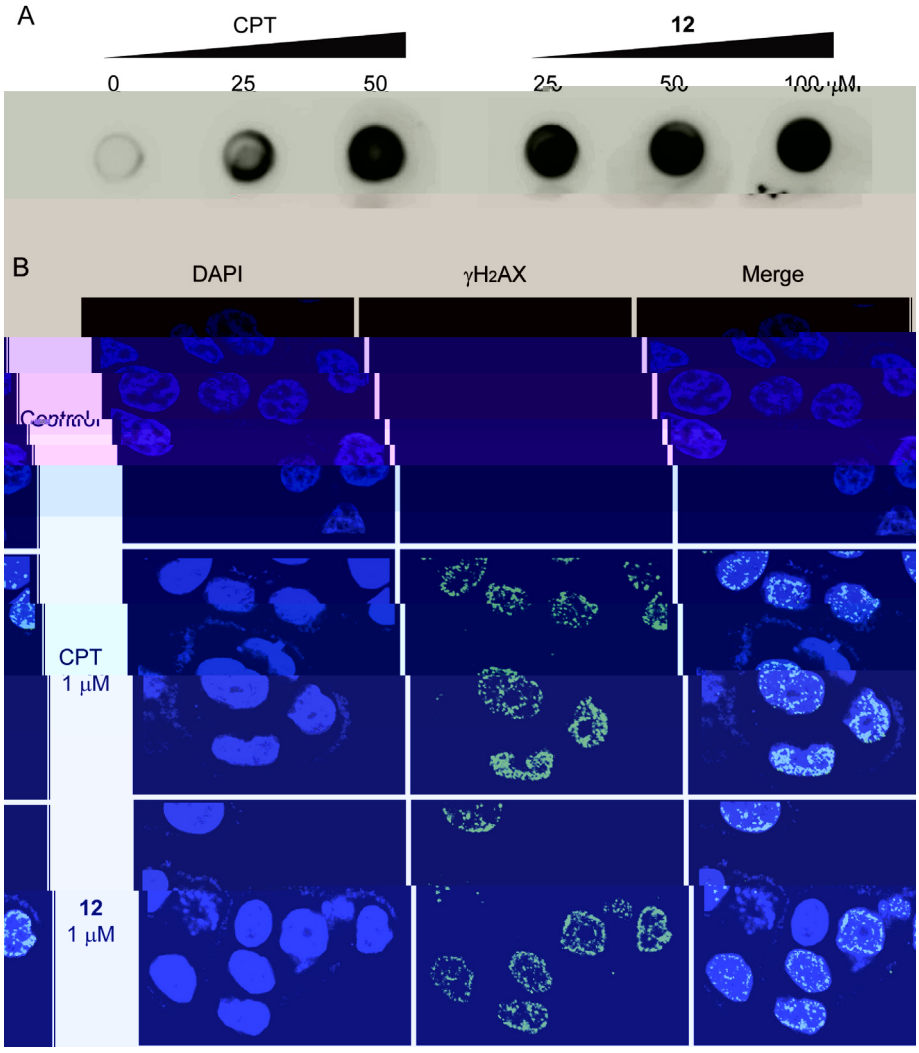

Fig. 4. (A) Detection of TOP1-DNA covalent cleavage complexes by *in vivo* complex of enzyme (ICE) assay in human colon cancer HCT116 cells. Left: lane 1, control; lanes 2 and 3, cells treated with CPT at 25 and 50 μM concentration, respectively. Right: lanes 1–3, cells treated with **12** at 25, 50 and 100 μM concentration, respectively. (B) Histone γH2AX foci induced by **12** in HCT116 cells. Cells were treated with CPT or **12** at 1 μM concentration for 3 h. DNA was stained with DAPI (blue). (For interpretation of the references to colour in this figure legend, the reader is referred to the Web version of this article.)

human colon cancer HCT116 and human breast cancer MCF-7 xenograft mude mice models. For both models, the mice were randomly divided into four groups (n = 6) and treated with **12** at 20 mg/kg, 10 mg/kg or 5 mg/kg dose by ip administration daily. The control group was treated with saline. As shown in Fig. 7, administration of **12** significantly reduced the tumor volume in a dose-dependent manner in both HCT116 and MCF-7 xenograft models. **12** is more antitumor efficient in HCT116 xenograft model than MCF-7 xenograft model. The tumor weight inhibitions (TWI) of **12** at 20 μM dose are 76.9% (in HCT116 model) and 71.8% (in MCF-7 model), respectively.

3. Conclusion

In summary, a series of novel 5-aminoethyl substituted benzophenanthridinone derivatives have been synthesized and evaluated for biochemical activity as TOP1 inhibitors and cellular responses against four human cancer cell lines (HCT116, MCF-7, DU145 and A549). The TOP1-mediated cleavage assay indicates that the derivatives with bigger termini of the side chain at the 5-position show decreased TOP1 inhibitory activity. Compound **12** with methylamino ethyl group at the 5-position exhibits the most potent TOP1 inhibition of +++, and cytotoxicity in human cancer cell lines at nanomolar concentration range GI_{50} values. **12** also shows consistent cytotoxicity in the NCI-60 cell lines with nanomolar MGM value of 0.0977 μM. Cell-based assays indicate that **12** induces the formation of cellular TOP1cc and DNA damage in HCT116 cells, promotes apoptosis, and is not a substrate of P-gp, a drug efflux protein responsible for multidrug resistance. **12** was also evaluated for PK, acute toxicity and antitumor efficiency *in vivo*. The results indicate that **12** exhibits antitumor efficiency in both HCT116 and MCF-7 xenograft nude mice models, and good bioavailability (20.4%) in rat model, higher than its analogue **2** (15.5%) with a dimethylaminoethyl group at 5-position, which might be the reason why **12** shows more potent antitumor activity both *in vitro* and *in vivo*. These results suggest that benzophenanthridinone scaffold is a chemotype for TOP1 inhibitors, and worth further development.

4. Experimental section

4.1. General experiments

All the required chemical reagents used for synthesis were

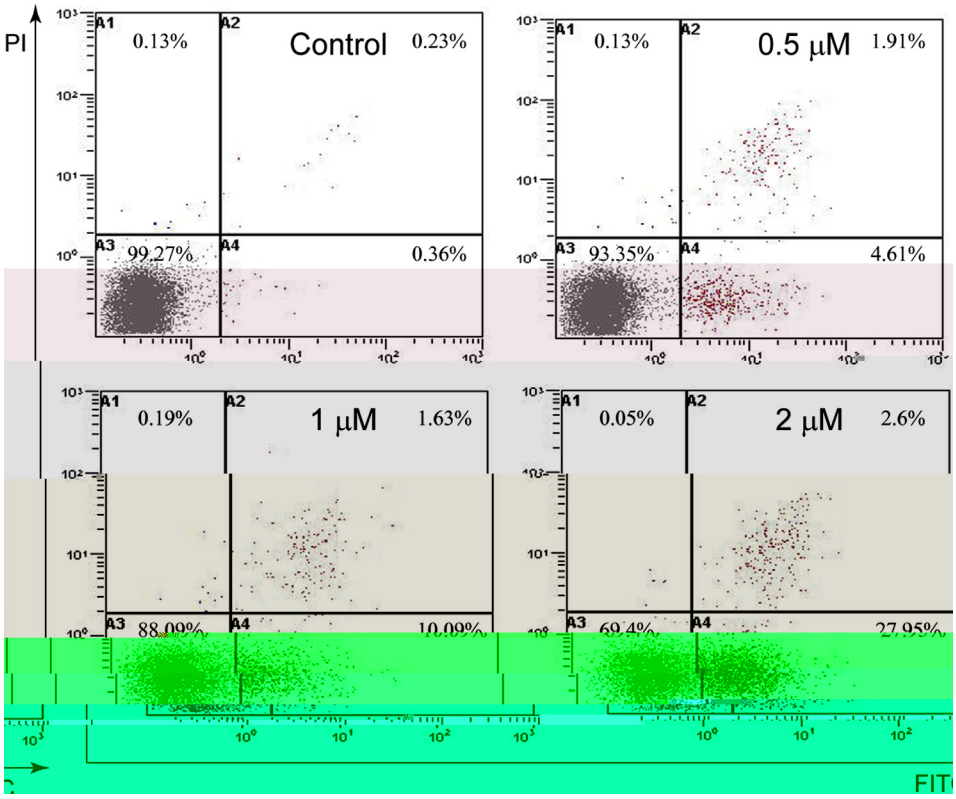

Fig. 5. Flow cytometry histograms. HCT116 cells were incubated with **12** for 24 h at 0.5 μM, 1 μM and 2 μM concentration, respectively.

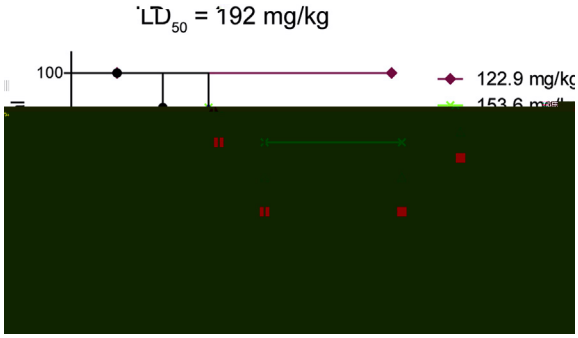

Fig. 6. Effect of **12** on mice survival. Mice were treated with **12** at dose 300 mg/kg, 240 mg/kg, 192 mg/kg 153.6 mg/kg and 122.9 mg/kg, respectively.

purchased from Sigma-Aldrich, Alfa Aesar or Aladdin Reagent Database Inc (Shanghai) and used without any further purification unless otherwise indicated. Melting points were determined in open capillary tubes on a MPA100 Optimelt Automated Melting Point System without being corrected. Silica gel GF_{254} thin layer chromatography (TLC) was used to monitor the progress of the chemical reaction. Nuclear magnetic resonance spectra were recorded on a Bruker AVANCE III 400 MHz spectrometer using tetramethylsilane as an internal reference. Mass spectra were analyzed on an Agilent 6120 (Quadrupole LC-MS) mass spectrometer. The high-resolution mass spectra were analyzed on an SHIMADZU LCMS-IT-TOF mass spectrometer. All compounds tested for biological activities were analyzed by HPLC and their purities were more than 95%. The analysis condition is: detection at 220 nm, 1.0 ml/min flow rate, a linear gradient of 50%–15% PBS buffer (pH 3) and 50%–85% MeOH in 35 min.

All animals were obtained from Laboratory Animal Center of Sun Yat-sen University. All procedures were approved by the Animal Ethics Committee of Sun Yat-sen University, in accordance with National Institute of Health and Nutrition Guidelines for the Care and Use of Laboratory Animals.

*4.2. 12-(2-bromoethyl)-2,3-dimethoxy-[1,3]dioxolo[4′,5':4,5]benzo [1,2-c]phenanthridin-13(12H)-one (**9**)*

To a solution of **8** (0.5 mmol) in freshly distilled chloroform (10 mL), PBr_3 (1 mL) was added slowly with a syringe. The mixture was stirred at room temperature for 1 h. The resulting gray precipitate was filtered and washed with chloroform, saturated sodium bicarbonate and water, respectively. The crude solid was dried and purified by silica gel column chromatography to give the gray solid **9**, yield 91%, ^{1}H NMR (DMSO) δ 8.84 (d, $J = 9.1$ Hz, 1H), 8.31 (s, 1H), 8.26 (s, 1H), 8.16 (d, $J = 9.0$ Hz, 1H), 7.73 (s, 1H), 7.69 (s, 1H), 6.33 (s, 2H), 5.76 (t, $J = 9.0$ Hz, 2H), 5.35 (t, $J = 9.0$ Hz, 2H), 4.21 (s, 3H), 4.04 (s, 3H). ESI-MS *m/z*: 455.1 (100%), 457.1 (100%) $[M + H]^+$.

*4.3. 12-(2-aminoethyl)-2,3-dimethoxy-[1,3]dioxolo[4′,5':4,5]benzo [1,2-c]phenanthridin-13(12H)-one (**11**)*

To a solution of **9** (456 mg, 1 mmol) in DMSO (50 mL), NaN_3 (130 mg, 2 mmol) was added. The mixture was stirred at room temperature for 16 h. And then, the reactive solution was poured into water (100 mL). The formed gray precipitate was filtered and washed with saturated sodium bicarbonate and water, respectively. The crude solid (**10**) was dried for the next synthesis without further purification.

The crude solid **10** was dissolved in THF (100 mL). Pd/C (42 mg) was added to the solution. The mixture was stirred at room

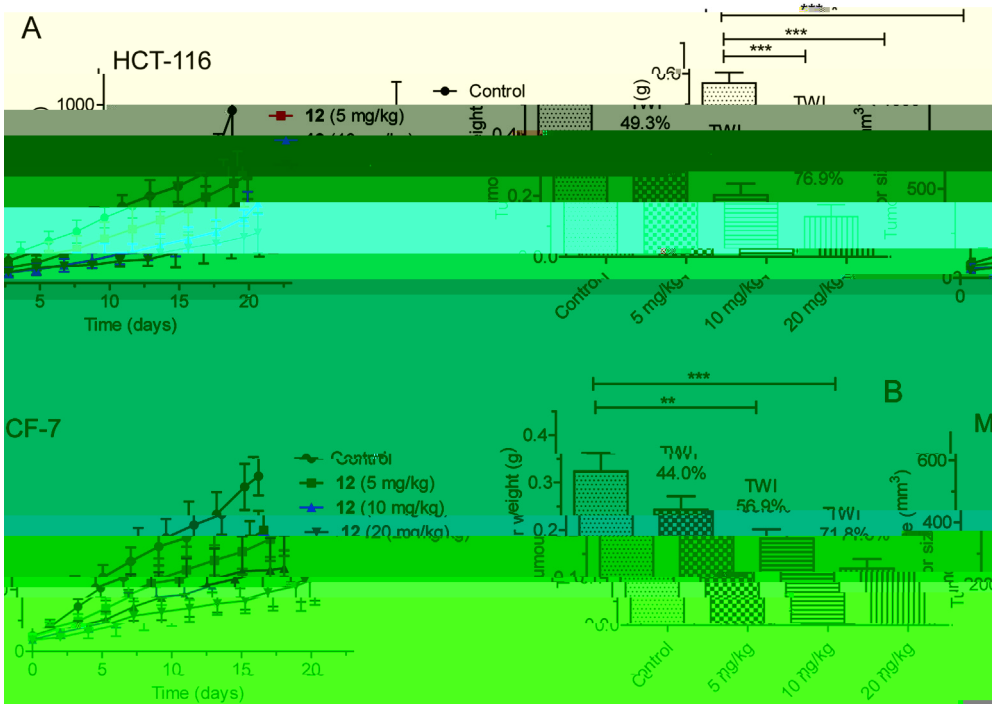

Fig. 7. Antitumor efficiency of **12** in HCT116 (A) and MCF-7 (B) xenograft models. The effects of **12** on tumor size (left) and tumor weight (right) at the dose of 5 mg/kg, 10 mg/kg and 20 mg/kg, respectively. Statistically significant difference in mean tumor weight compared with the control, **: $P < 0.01$, ***: $P < 0.001$.

temperature under hydrogen atmosphere for 2 h. The reaction mixture was filtered and washed with THF. The filtrate was dried over $MgSO_4$ and concentrated under reduced pressure. The residue was purified by silica gel column chromatography to give the white solid **11**, yield 51% for the two steps, mp = 264.3–267.1 °C. ^{1}H NMR ($CDCl_3$) δ 7.98 (d, J = 8.4 Hz, 1H), 7.91 (s, 1H), 7.59–7.54 (m, 2H), 7.52 (s, 1H), 7.18 (s, 1H), 6.10 (s, 2H), 4.60 (t, J = 6.0 Hz, 2H), 4.11 (s, 3H), 4.06 (s, 3H), 3.13 (t, J = 6.0 Hz, 2H). ^{13}C NMR ($CDCl_3$) δ 164.9, 153.8, 149.9, 147.7, 147.6, 135.6, 131.9, 129.1, 123.6, 121.3, 119.6, 118.5, 117.4, 109.0, 105.0, 103.0, 102.4, 101.7, 56.4, 56.3, 55.1, 41.5. HRMS (ESI) *m/z*: 393.1439 $[M + H]^+$, calcd for $C_{22}H_{21}N_2O_5$ 393.1445.

4.4. 2,3-Dimethoxy-12-(2-(methylamino)ethyl)-[1,3]dioxolo [4′,5′:4,5]benzo[1,2-c]phenanthridin-13(12H)-one (12)

To a solution of **11** (470 mg, 0.12 mmol) in acetic acid (140 mL) and water (100 mL), aqueous formaldehyde solution (40%, 90 mL) and Zn (156 mg, 2.4 mmol) was added. The mixture was stirred at room temperature overnight. Ammonia water was added to quench the reaction. The solution was exacted with chloroform (3 x 50 mL). The combined organic layer was dried over $MgSO_4$ and concentrated under reduced pressure. The residue was purified by silica gel column chromatography to give the white solid **12**, yield 59%, mp = 211.8–212.0 °C. ^{1}H NMR ($CDCl_3$) δ 7.97 (d, J = 8.8 Hz, 1H), 7.90 (s, 1H), 7.59–7.54 (m, 2H), 7.54 (s, 1H), 7.18 (s, 1H), 6.10 (s, 2H), 4.61 (t, J = 6.4 Hz, 2H), 4.10 (s, 3H), 4.05 (s, 3H), 3.11 (t, J = 6.4 Hz, 2H), 2.36 (s, 3H). ^{13}C NMR ($CDCl_3$) δ 165.0, 153.9, 149.9, 147.7, 147.6, 135.6, 131.9, 129.2, 123.6, 121.2, 119.6, 118.5, 117.4, 108.9, 105.0, 103.1, 102.4, 101.7, 56.4, 56.3, 52.0, 51.3, 36.2. HRMS (ESI) *m/z*: 407.1601 $[M + H]^+$,calcd for $C_{23}H_{23}N_2O_5$ 407.1601.

4.5. General procedure for the synthesis of compounds 13–25

To a solution of **12** (or **11**, 0.24 mmol) and DIPEA (2.4 mmol) in freshly distilled dichloromethane (30 mL), the solution of acyl chlorides (0.32 mmol) in dichloromethane (5 mL) was added slowly at an ice bath. And then, the reaction solution was stirred and heated under reflux for 1 h (for **13**–**19**, or at room temperature for **20**–**25**). The reaction solution was cooled to room temperature. The solvent was evaporated under reduced pressure. The residue was purified by silica gel column chromatography to give target product.

4.5.1. N-(2-(2,3-dimethoxy-13-oxo-[1,3]dioxolo[4′,5′:4,5]benzo[1,2-c]phenan-thridin-12(13H)-yl)ethyl)-1,1,1-trifluoro-N-methylmethanesulfonamide (13)

White solid, yield 40%, mp = 217.4–217.8 °C. ^{1}H NMR ($CDCl_3$) δ 7.99 (d, J = 8.8 Hz, 1H), 7.87 (s, 1H), 7.62–7.56 (m, 2H), 7.41 (s, 1H), 7.20 (s, 1H), 6.13 (s, 2H), 4.81 (t, J = 6.6 Hz, 2H), 4.11 (s, 2H), 4.06 (s, 2H), 3.82 (s, 2H), 2.87 (s, 3H). ^{13}C NMR ($CDCl_3$) δ 164.6, 153.9, 149.8, 147.8, 147.7, 134.6, 131.8, 129.2, 123.9, 120.5, 119.2, 118.4, 117.7, 108.6, 105.2, 102.9, 101.7, 101.6, 56.2, 56.2, 49.0, 48.8, 35.9. HRMS (ESI) *m/z*: 539.1116 $[M + H]^+$, calcd for $C_{24}H_{22}N_2O_7F_3S$ 539.1094.

4.5.2. N-(2-(2,3-dimethoxy-13-oxo-[1,3]dioxolo[4′,5′:4,5]benzo [1,2-c]phenanth-ridin-12(13H)-yl)ethyl)-N-methylcyclopropanesulfonamide (14)

White solid, yield 80%, mp > 280 °C. ^{1}H NMR ($CDCl_3$) δ 7.96 (d, J = 8.5 Hz, 1H), 7.88 (s, 1H), 7.56 (d, J = 6.0 Hz, 2H), 7.52 (s, 1H), 7.17 (s, 1H), 6.11 (s, 2H), 4.74 (t, J = 6.5 Hz, 2H), 4.10 (s, 2H), 4.05 (s, 2H), 3.74 (t, J = 6.6 Hz, 2H), 2.78 (s, 3H), 2.08 (d, J = 4.5 Hz, 1H), 1.07 (d, J = 3.6 Hz, 2H), 0.83 (d, J = 6.2 Hz, 2H). ^{13}C NMR ($CDCl_3$) δ 164.6, 153.8, 149.7, 147.7, 147.7, 135.1, 131.8, 129.2, 123.7, 120.7, 119.2, 118.3, 117.4, 108.6, 104.9, 102.9, 102.1, 101.7, 56.2, 56.1, 50.2, 48.5, 35.7, 26.9, 4.5, 4.5. HRMS (ESI) *m/z*: 511.1536 $[M + H]^+$, calcd for $C_{26}H_{27}N_2O_7S$ 511.1533.

4.5.3. N-(2-(2,3-dimethoxy-13-oxo-[1,3]dioxolo[4′,5′:4,5]benzo [1,2-c]phenan-thridin-12(13H)-yl)ethyl)-N-methyldimethylamine-1-sulfonamide (15)

White solid, yield 83%, mp = 234.7–235.9 °C·^{1}H NMR ($CDCl_3$)

δ 7.97 (d, J = 8.6 Hz, 1H), 7.88 (s, 1H), 7.60−7.49 (m, 3H), 7.18 (s, 1H), 6.12 (s, 2H), 4.74 (t, J = 6.5 Hz, 2H), 4.11 (s, 3H), 4.05 (s, 3H), 3.71 (t, J = 6.5 Hz, 2H), 2.68 (s, 3H), 2.59 (s, 6H). ^{13}C NMR ($CDCl_3$) δ 164.6, 153.8, 149.7, 147.7, 147.6, 135.2, 131.8, 129.2, 123.6, 120.8, 119.3, 118.3, 117.4, 108.6, 104.9, 102.8, 102.1, 101.7, 56.3, 56.2, 49.8, 48.9, 37.8, 37.8, 36.1. HRMS (ESI) *m/z*: 514.1669 $[M + H]^+$, calcd for $C_{25}H_{28}N_3O_7S$ 514.1642.

4.5.4. N-(2-(2,3-dimethoxy-13-oxo-[1,3]dioxolo[4′,5':4,5]benzo [1,2-c]phena-nthridin-12(13H)-yl)ethyl)-N-methylpyrrolidine-1-sulfonamide (**16**)

White solid, yield 81%, mp = 223.4−224.3 °C. ^{1}H NMR ($CDCl_3$) δ 7.97 (d, J = 8.7 Hz, 1H), 7.89 (s, 1H), 7.56 (d, J = 6.5 Hz, 2H), 7.54 (s, 1H), 7.18 (s, 1H), 6.12 (s, 2H), 4.75 (t, J = 6.6 Hz, 2H), 4.11 (s, 3H), 4.05 (s, 3H), 3.69 (t, J = 6.6 Hz, 2H), 3.03 (t, J = 6.7 Hz, 4H), 2.64 (s, 3H), 1.82−1.75 (m, 4H). ^{13}C NMR ($CDCl_3$) δ 164.6, 153.8, 149.7, 147.7, 147.6, 135.3, 131.8, 129.2, 123.5, 120.9, 119.4, 118.2, 117.4, 108.7, 104.9, 102.9, 102.2, 101.7, 56.3, 56.2, 50.1, 48.8, 47.9, 47.9, 35.9, 25.5, 25.5. HRMS (ESI) *m/z*: 540.1811 $[M + H]^+$, calcd for $C_{27}H_{30}N_3O_7$ 540.1799.

4.5.5. N-(2-(2,3-dimethoxy-13-oxo-[1,3]dioxolo[4′,5':4,5]benzo [1,2-c]phenan-thridin-12(13H)-yl)ethyl)-N-methylmorpholine-4-sulfonamide (**17**)

White solid, yield 85%, mp = 205.7−206.2 °C. ^{1}H NMR ($CDCl_3$) δ 7.96 (d, J = 8.7 Hz, 1H), 7.88 (s, 1H), 7.56 (t, J = 4.3 Hz, 2H), 7.27 (s, 1H), 7.17 (s, 1H), 6.11 (s, 2H), 4.75 (t, J = 6.5 Hz, 2H), 4.11 (s, 3H), 4.06 (s, 3H), 3.69 (t, J = 6.5 Hz, 2H), 3.55 (t, J = 4.0 Hz, 4H), 2.91(t, J = 4.0 Hz, 3H), 2.64 (s, 3H). ^{13}C NMR ($CDCl_3$) δ 164.5, 153.8, 149.8, 147.7, 147.7, 135.1, 131.7, 129.1, 123.6, 120.8, 119.3, 118.3, 117.5, 108.6, 104.9, 102.8, 102.1, 101.7, 66.2, 66.2, 56.5, 56.2, 49.9, 48.9, 45.9, 45.9, 36.3. HRMS (ESI) *m/z*: 556.1778 $[M + H]^+$, calcd for $C_{27}H_{30}N_3O_8S$ 556.1748.

4.5.6. Dimethyl(2-(2,3-dimethoxy-13-oxo-[1,3]dioxolo[4′,5':4,5] benzo[1,2-c]phe-nanthridin-12(13H)-yl)ethyl)(methyl) phosphoramidate (**18**)

White solid, yield 30%, mp = 220.0−221.7 °C. ^{1}H NMR ($CDCl_3$) δ 7.97 (d, J = 8.6 Hz, 1H), 7.90 (s, 1H), 7.57 (s, 1H), 7.54 (d, J = 5.9 Hz, 2H), 7.18 (s, 1H), 6.11 (s, 2H), 4.73 (t, J = 6.5 Hz, 2H), 4.10 (s, 3H), 4.06 (s, 3H), 3.55−3.47 (m, 2H), 3.44 (s, 3H), 3.42 (s, 3H), 2.49 (d, J = 9.8 Hz, 3H). ^{13}C NMR ($CDCl_3$) δ 164.5, 153.6, 149.7, 147.6, 147.5, 135.3, 131.7, 129.1, 123.4, 120.9, 119.4, 118.3, 117.4, 108.8, 104.8, 102.8, 102.3, 101.6, 56.3, 56.1, 52.7, 52.7, 50.3, 47.4, 34.3. HRMS (ESI) *m/z*: 515.1584 $[M + H]^+$, calcd for $C_{25}H_{28}N_2O_8P$ 515.1578.

4.5.7. 2,3-Dimethoxy-12-(2-(methyl(2-oxido-1,3,2-dioxaphospholan-2-yl)amino)ethyl)-[1,3]dioxolo[4′,5':4,5]benzo [1,2-c]phenanthridin-13(12H)-one (**19**)

White solid, yield 40%, mp = 221.3−222.4 °C. ^{1}H NMR ($CDCl_3$) δ 7.97 (d, J = 8.8 Hz, 1H), 7.86 (s, 1H), 7.56 (dd, J = 11.7, 6.9 Hz, 2H), 7.51 (s, 1H), 7.18 (s, 1H), 6.12 (s, 2H), 4.74−4.66 (m, 2H), 4.32−4.25 (m, 2H), 4.24−4.19 (m, 2H), 4.11 (s, 3H), 4.05 (s, 3H), 3.53−3.41 (m, 2H), 2.65 (d, J = 10.2 Hz, 2H). ^{13}C NMR ($CDCl_3$) δ 164.6, 153.6, 149.6, 147.6, 147.5, 135.0, 131.7, 129.2, 123.5, 120.7, 119.3, 118.3, 117.5, 108.5, 104.9, 102.9, 102.0, 101.7, 65.7, 65.6, 56.3, 56.1, 49.1, 47.0, 34.5. HRMS (ESI) *m/z*: 513.1446 $[M + H]^+$, calcd for $C_{25}H_{36}N_2O_8P$ 513.1421.

4.5.8. N-(2-(2,3-dimethoxy-13-oxo-[1,3]dioxolo[4′,5':4,5]benzo [1,2-c]phenanthridin-12(13H)-yl)ethyl)cyclopropanesulfonamide (**20**)

White solid, yield 60%, mp = 245.4−246.2 °C. ^{1}H NMR $CDCl_3$) δ 7.97 (d, J = 8.7 Hz, 1H), 7.86 (s, 1H), 7.57 (d, J = 9.7 Hz, 2H), 7.30 (s, 1H), 7.18 (s, 1H), 6.12 (s, 2H), 5.52 (t, J = 6.1 Hz, 1H), 4.62 (t, J = 5.5 Hz, 2H), 4.11 (s, 3H), 4.05 (s, 3H), 3.78 (dd, J = 11.4, 5.7 Hz, 2H), 2.26 (td, J = 8.0, 4.1 Hz, 1H), 1.14−1.02 (m, 2H), 0.92−0.81 (m, 2H). ^{13}C NMR ($CDCl_3$) δ 165.0, 153.9, 149.8, 147.7, 147.6, 135.1, 131.8, 129.2, 123.7, 120.7, 118.9, 118.4, 117.3, 108.6, 105.1, 102.9, 101.7, 101.7, 56.3, 56.2, 52.6, 43.5, 30.2, 5.4, 5.4. HRMS (ESI) *m/z*: 497.1394 $[M + H]^+$, calcd for $C_{25}H_{25}N_2O_7S$ 497.1377.

4.5.9. N-(2-(2,3-dimethoxy-13-oxo-[1,3]dioxolo[4′,5':4,5]benzo [1,2-c]phenanthridin-12(13H)-yl)ethyl)dimethylamine-1-sulfonamide (**21**)

White solid, yield 65%, mp > 280 °C. ^{1}H NMR ($CDCl_3$) δ 7.98 (d, J = 8.7 Hz, 1H), 7.86 (s, 1H), 7.57 (d, J = 8.0 Hz, 2H), 7.29 (s, 1H), 7.19 (s, 1H), 6.11 (s, 2H), 5.58 (t, J = 5.9 Hz, 1H), 4.59 (t, J = 5.4 Hz, 2H), 4.11 (s, 3H), 4.06 (s, 3H), 3.70 (t, J = 5.4 Hz, 2H), 2.70 (s, 6H). ^{13}C NMR ($CDCl_3$) δ 165.1, 153.9, 149.8, 147.7, 147.6, 135.1, 131.9, 129.2, 123.8, 120.7, 118.9, 118.4, 117.3, 108.6, 105.1, 102.9, 101.7, 101.7, 56.3, 56.2, 52.4, 44.2, 37.9. 37.9. HRMS (ESI) *m/z*: 500.1531 $[M + H]^+$, calcd for $C_{24}H_{26}N_3O_7S$ 500.1486.

4.5.10. N-(2-(2,3-dimethoxy-13-oxo-[1,3]dioxolo[4′,5':4,5]benzo [1,2-c]phenanthridin-12(13H)-yl)ethyl)pyrrolidine-1-sulfonamide (**22**)

White solid, yield 85%, mp = 249.7−250.8 °C. ^{1}H NMR ($CDCl_3$) δ 7.98 (d, J = 8.7 Hz, 1H), 7.87 (s, 1H), 7.58 (d, J = 7.2 Hz, 2H), 7.31 (s, 1H), 7.19 (s, 1H), 6.12 (s, 2H), 5.41 (t, J = 5.9 Hz, 1H), 4.62 (t, J = 5.4 Hz, 2H), 4.11 (s, 3H), 4.06 (s, 3H), 3.70−3.67 (m, 2H), 3.19 (t, J = 6.6 Hz, 4H), 1.82 (t, J = 6.6 Hz, 4H). ^{13}C NMR ($CDCl_3$) δ 165.0, 153.9, 149.8, 147.6, 147.6, 135.2, 131.9, 129.2, 123.7, 120.8, 119.1, 118.4, 117.4, 108.7, 105.1, 102.9, 101.8, 101.7, 56.3, 56.2, 52.3, 48.0, 48.0, 43.9, 25.5, 25.5. HRMS (ESI) *m/z*: 526.1640 $[M + H]^+$, calcd for $C_{26}H_{28}N_3O_7S$ 526.1642.

4.5.11. N-(2-(2,3-dimethoxy-13-oxo-[1,3]dioxolo[4′,5':4,5]benzo [1,2-c]phenanthridin-12(13H)-yl)ethyl)morpholine-4-sulfonamide (**23**)

White solid, yield 70%, mp = 221.6−222.3 °C. ^{1}H NMR ($CDCl_3$) δ 7.98 (d, J = 8.5 Hz, 1H), 7.85 (s, 1H), 7.58 (d, J = 11.4 Hz, 2H), 7.27 (s, 1H), 7.19 (s, 1H), 6.12 (s, 2H), 5.66 (s, 1H), 4.61 (t, J = 4.8 Hz 2H), 4.11 (s, 3H), 4.06 (s, 3H), 3.68 (t, J = 4.8 Hz, 2H), 3.64 (s, 4H), 3.06 (s, 4H). ^{13}C NMR ($CDCl_3$) δ 165.2, 154.0, 149.9, 147.7, 147.7, 135.0, 131.9, 129.2, 123.8, 120.7, 118.9, 118.4, 117.4, 108.6, 105.1, 102.9, 101.7, 101.6, 66.1, 66.1, 56.3, 56.2, 52.3, 46.1, 44.4, 44.4. HRMS (ESI) *m/z*: 542.1623 $[M + H]^+$, calcd for $C_{26}H_{28}N_3O_8S$ 542.1592.

4.5.12. Dimethyl(2-(2,3-dimethoxy-13-oxo-[1,3]dioxolo[4′,5':4,5] benzo[1,2-c]phena-nthridin-12(13H)-yl)ethyl)phosphoramidate (**24**)

White solid, yield 62%, mp = 197.2−197.8 °C. ^{1}H NMR ($CDCl_3$) δ 7.97 (d, J = 8.7 Hz, 1H), 7.88 (s, 1H), 7.56 (d, J = 7.5 Hz, 2H), 7.37 (s, 1H), 7.19 (s, 1H), 6.11 (s, 2H), 4.60 (t, J = 5.8 Hz, 2H), 4.11 (s, 3H), 4.06 (s, 3H), 3.55 (s, 3H), 3.52 (s, 3H), 3.50−3.46 (m, 2H). ^{13}C NMR ($CDCl_3$) δ 164.8, 153.8, 149.8, 147.6, 147.5, 135.4, 131.7, 129.1, 123.6, 120.9, 119.3, 118.4, 117.3, 108.7, 104.9, 102.9, 101.9, 101.6, 56.3, 56.2, 53.6, 52.9, 52.9, 41.1. HRMS (ESI) *m/z*: 501.1423 $[M + H]^+$, calcd for $C_{24}H_{26}N_2O_8P$ 501.1421.

4.5.13. N-(2-(2,3-dimethoxy-13-oxo-[1,3]dioxolo[4′,5':4,5]benzo [1,2-c]phena-nthridin-12(13H)-yl)ethyl)cyclopropanecarboxamide (**25**)

White solid, yield 80%, mp = 237.6−238.1 °C. ^{1}H NMR ($CDCl_3$) δ 7.97 (d, J = 8.7 Hz, 1H), 7.89 (s, 1H), 7.57 (d, J = 9.7 Hz, 2H), 7.42 (s, 1H), 7.17 (s, 1H), 6.73 (s, 1H), 6.10 (s, 2H), 4.60 (t, J = 4.9 Hz, 2H), 4.11 (s, 3H), 4.07 (s, 3H), 3.88 (d, J = 5.0 Hz, 2H), 0.87 (d, J = 6.7 Hz, 1H), 0.81 (s, 2H), 0.63 (d, J = 4.7 Hz, 2H). ^{13}C NMR ($CDCl_3$) δ 173.5, 165.2, 153.8, 149.7, 147.7, 147.6, 135.4, 131.8, 129.3, 123.7, 120.9, 119.1, 118.2, 117.1, 108.5, 104.9, 102.9, 102.1, 101.7, 56.3, 56.2, 52.2, 40.3, 14.7, 7.0, 7.0. HRMS (ESI) *m/z*: 461.1732 $[M + H]^+$, calcd for $C_{26}H_{25}N_2O_6$

461.1707.

4.6. TOP1-mediated cleavage assay

DNA cleavage assays were performed using a 3'-[^{32}P]-labeled 117-bp DNA oligonucleotide as substrate according to the previously reported method [26]. Approximately 2 nM radiolabeled DNA substrate was incubated with recombinant TOP1 in 20 mL of reaction buffer (10 mM Tris-HCl pH 7.5, 50 mM KCl, 5 mM $MgCl_2$, 0.1 mM EDTA, and 15 mg/mL BSA) at 25 °C for 20 min in the presence of various concentrations of test compounds. The reactions were terminated by adding SDS (0.5% final concentration) followed by the addition of two volumes of loading dye (80% formamide, 10 mM sodium hydroxide, 1 mM sodium EDTA, 0.1% xylene cyanol, and 0.1% bromophenol blue). Aliquots of each reaction mixture were subjected to 20% denaturing PAGE. Gels were dried and visualized by using a phosphoimager and ImageQuant software (Molecular Dynamics). Cleavage sites are numbered to reflect actual sites on the 117-bp oligonucleotide.

4.7. Molecular modelling

The molecular modelling was conducted as previously reported method [22]. Briefly, the X-ray crystal structures of the ternary TOP1-DNA-ligand complex (PDB ID: 1K4T) was obtained and cleaned, inspected for errors and missing residues, hydrogens were added, and the water molecules and the ligand were deleted. The ternary complex ligand centroid coordinates for docking were defined using the ligand in the complex structure as the center of the binding pocket. The compounds constructed using ChemDraw were saved in SDFfile formats and corrected using MOE software. The top 30 docking poses per ligand were inspected visually following the docking runs. The highest-ranked poses for these ligands were merged into the crystal structure. Energy minimizations were performed for the highest-ranked poses for these ligands. The AMBER forcefield was utilized within the MOE software for energy minimization.

4.8. Cell culture and MTT assay

The cells were cultured on RPMI-1640 medium at 37 °C in a humidified atmosphere with 5% CO_2. All cells to be tested in the following assays had a passage number of 3–6. For the drug treatment experiments, the cancer cells were treated with the compounds (predissolved in DMSO) at a five-dose assay ranging from 0.01 to 100 μM concentration. After incubation for 72 h at 37 °C, MTT solution (50 μL, 1 mg/mL) in PBS (PBS without MTT as the blank) was fed to each well of the culture plate (containing 100 mL medium). After 4 h incubation, the formazan crystal formed in the well was dissolved with 100 mL of DMSO for optical density reading at 570 nm [35]. The GI_{50} value was calculated by nonlinear regression analysis (GraphPad Prism).

4.9. Immunodetection of cellular TOP1-DNA complex

The ICE assays for cellular TOP1-DNA adduct was performed according to the reported method [36]. Briefly, mid-log phase HCT-116 cells were incubated with drugs at the indicated concentration for 1 h. And then, the cells were lysed with DNAzol Reagent (1 mL) at 25 °C for 30 min. Ethanol (0.5 ml, 100%) was subsequently added and mixed with the lysate and the solution was incubated overnight at −20 °C. The genomic DNA was collected by centrifugation (12,000 rpm) at 25 °C for 10 min and washed with 75% ethanol. The precipitated DNA was dissolved in NaOH (8 mM, 0.2 ml). The pH value was adjusted to 7.2 by adding HEPES (1 M). After centrifugation, supernatant was used to quantify the DNA concentration. DNA (2 μg) were dissolved in NaH_2PO_4 buffer (30 μL, 25 mM, pH 6.5) and then loaded onto nitrocellulose membranes. Membranes were incubated with rabbit monoclonal to human TOP1 (Abcam, 1:1000) overnight at 4 °C, and then incubated with the appropriate HRPconjugated secondary antibodies (Cell Signaling Technology, 1:3000) at room temperature for 1 h. Reactive dots were detected using Immobilon Western Chemiluminescent HRP Substrate (Millipore).

4.10. γH2AX detection

γH2AX staining was performed as described [37]. Briefly, HCT116 cells (2×10^4 cells/mL) were grown in culture medium and treated with compounds for 3 h at 37 °C. After incubation, cells were fixed in 4% paraformaldehyde/PBS for 15 min at 25 °C and washed three times with PBS buffer. Cells were permeabilized with 0.5% Triton X-100 in PBS at 0 °C for 30 min. Dish was blocked with 5% goat serum/PBS at 37 °C for 3 h. Immunofluorescence assay was performed using standard methods, and the slides were incubated alternately with phospho-γH2AX (Cell Signaling Technology) at 37 °C overnight. The cover slips were washed six times with blocking buffer and then incubated with anti-rabbit alexa 488-conjugated antibody (A21206, Life Technology) and 2.0 μg/mL of 4′,6-diamidino-2-phenylindole (DAPI, Invitrogen) at 37 °C for 2 h. The dishes were again washed six times with blocking buffer. Digital images were recorded using an LSM710 microscope (Zeiss, Germany) and analyzed with ZEN software.

4.11. Pharmacokinetic study in vivo

The PK study was conducted according to our previous method [22]. Briefly, male SD rats (weighing 220–250 g, n = 2) were treated with compound **12** pre-dissolved in10% DMSO and 10% Kolliphor® HS15 (a non-ionic solubilizer) by iv (1 mg/kg) and by ig administration (5 mg/kg), respectively. Blood samples (200 μL) were collected into heparinized tubes via the jugular vein at the following times: 0.083, 0.25, 0.5, 1, 2 and 4 h after dosing. Plasma samples (100 μL) were obtained after centrifugation for 10 min at 3000 rpm and stored at −20 °C until used for analysis. The plasma was detected through LC-MS-MS.

4.12. In vivo acute toxicity

Based on the preliminary experiments, the Kuning male mice were randomly divided into six groups (n = 6) and administered by intraperitoneal (ip) injection. The control group was treated with an equivalent volume of sterile water. The testing groups were treated with compound **12** in a single dose 300, 240, 192, 153.6 and 122.9 mg/kg, respectively. The mice were kept under observation for 7 days post-treatment in order to check for any behavioral (poisoning symptoms and body weight) and death. All animals were euthanized by cervical dislocation at the end of the experiments.

4.13. In vivo antitumor activity

Athymic nude mice bearing the nu/nu gene were obtained from Laboratory Animal Center of Sun Yat-sen University and maintained in pathogen-free conditions to establish the model of xenografts of HCT116 and MCF-7. Male nude mice 4–5 weeks old weighing 12–15 g were used. Tumor pre-induced in the mice by subcutaneously injecting of cancer cells (100 μL, 1×10^7 cells) was implanted. When the implanted tumors had reached a volume of about 80 mm^3, the mice were randomly divided into four groups

(n = 6) and administered by intraperitoneal injection. The testing groups were treated with **12** in 20 mg/kg, 10 mg/kg and 5 mg/kg dose once every day, respectively. The negative control group was treated with an equivalent volume of saline. Tumor volumes (V) were monitored by caliper measurement of the length and width, and calculated using the formula: V = (larger diameter) × (smaller diameter)^2/2, and growth curves were plotted using average tumor volume within each experimental group at the set time points. At the end of the experiment, the animals were euthanized by cervical dislocation. The tumors were removed and weighed. The tumor weight inhibition (TWI) was calculated according to the formula: TWI = (1-Mean tumor weight of the experimental group/Mean tumor weight of the control group) × 100%.

4.14. Statisticl analysis

All data are expressed as the mean ± standard deviation. Statistical comparisons were conducted using a one-way analysis of variance (ANOVA) using the Prism statistical software package (GraphPad Software, USA), followed by Tukey's test.

Acknowledgement

This work was supported by the National Natural Science Foundation of China (No. 81373257), Natural Science Foundation of Guangdong Province (No. S2013010015609), Guangdong Provincial Key Laboratory of Construction Foundation (No. 2017B030314030) and supported by the Intramural Program of the National Cancer Institute (Center for Cancer Research), National Institutes of Health, Bethesda, Maryland, USA (Z01 BC 006150-19 and Z01 BC006161-171).

Appendix A. Supplementary data

Supplementary data to this article can be found online at https://doi.org/10.1016/j.ejmech.2019.05.074.

References

[1] J.C. Wang, DNA topoisomerases, Annu. Rev. Biochem. 65 (1996) 635–692.
[2] L. Stewart, M.R. Redinbo, X. Qui, W.G.J. Hol, J.J. Champoux, A model for the mechanism of human topoisomerase I, Science 279 (1998) 1534–1541.
[3] J.J. Champoux, DNA topoisomerases: structure, function, and mechanism, Annu. Rev. Biochem. 70 (2001) 369–413.
[4] Y. Pommier, E. Leo, H. Zhang, C. Marchand, DNA topoisomerases and their poisoning by anticancer and antibacterial drugs, Chem. Biol. 17 (2010) 421–433.
[5] Y. Pommier, Y. Sun, S.N. Huang, J.L. Nitiss, Roles of eukaryotic topoisomerases in transcription, replication and genomic stability, Nat. Rev. Mol. Cell Biol. 17 (2016) 703–721.
[6] Y. Pommier, DNA topoisomerase I inhibitors: chemistry, biology, and interfacial inhibition, Chem. Rev. 109 (2009) 2894–2902.
[7] B.L. Staker, K. Hjerrild, M.D. Feese, C.A. Behnke, A.B. Burgin Jr., L. Stewart, The mechanism of topoisomerase I poisoning by a camptothecin analog, Proc. Natl. Acad. Sci. U. S. A. 99 (2002) 15387–15392.
[8] B.L. Staker, M.D. Feese, M. Cushman, Y. Pommier, D. Zembower, L. Stewart, A.B. Burgin, Structures of three classes of anticancer agents bound to the human topoisomerase I-DNA covalent complex, J. Med. Chem. 48 (2005) 2336–2345.
[9] Y. Pommier, Topoisomerase I inhibitors: camptothecins and beyond, Nat. Rev. Canc. 6 (2006) 789–802.
[10] G.L. Beretta, P. Perego, F. Zunino, Targeting topoisomerase I: molecular mechanisms and cellular determinants of response to topoisomerase I inhibitors, Expert Opin. Ther. Targets 12 (2008) 1243–1256.
[11] S.-H. Choi, Y. Tsuchida, H.-W. Yang, Oral versus intraperitoneal administration of irinotecan in the treatment of human neuroblastoma in nude mice, Cancer Lett. 124 (1998) 15–21.
[12] R.N. Brogden, L.R. Wiseman, Topotecan a review of its potential in advanced ovarian cancer, Drugs 56 (1998) 709–723.
[13] F. Bracher, T. Tremmel, From lead to drug utilizing a mannich reaction: the topotecan story, Arch. Pharm. Chem. Life Sci. 350 (2017), e1600236.
[14] R. Zhang, Y. Li, Q. Cai, T. Liu, H. Sun, B. Chambless, Preclinical pharmacology of the natural product anticancer agent 10-hydroxycamptothecin, an inhibitor of topoisomerase I, Cancer Chemother, Pharmacologist 41 (1998) 257–267.
[15] S. Jianghe, H. Fengming, F. Jianwei, Clinical study on treatment of non-small cell lung cancer with 10-hydroxycamptothecin, Chin. J. Clin. Oncol. 30 (2003) 26–28.
[16] S.J. Kim, J.S. Kim, S.C. Kim, Y.K. Kim, Y.K. Kim, J.Y. Kang, H.K. Yoon, J.S. Song, S.H. Lee, H.S. Moon, J.W. Kim, K.H. Kim, C.H. Kim, B.Y. Shim, H.K. Kim, A multicenter phase II study of belotecan, new camptothecin analogue, in patients with previously untreated extensive stage disease small cell lung cancer, Lung Cancer 68 (2010) 446–449.
[17] Q. Lian, J. Xu, S. Yan, M. Huang, H. Ding, X. Sun, A. Bi, J. Ding, B. Sun, M. Geng, Chemotherapy-induced intestinal inflammatory responses are mediated by exosome secretion of double-strand DNA via AIM2 inflammasome activation, Cell Res. 27 (2017) 784–800.
[18] T.-K. Li, P.J. Houghton, S.D. Desai, P. Daroui, A.A. Liu, E.S. Hars, A.L. Ruchelman, E.J. LaVoie, L.F. Liu, Characterization of ARC-111 as a novel topoisomerase I-targeting anticancer drug, Cancer Res. 63 (2003) 8400–8407.
[19] J.H. Burton, C.N. Mazcko, A.K. LeBlanc, J.M. Covey, J.J. Ji, R.J. Kinders, R.E. Parchment, C. Khanna, M. Paoloni, S.E. Lana, K. Weishaar, C.A. London, W.C. Kisseberth, E. Krick, D.M. Vail, M.O. Childress, J.N. Bryan, L.G. Barber, E.J. Ehrhart, M.S. Kent, T.M. Fan, K.Y. Kow, N. Northup, H. Wilson-Robles, J.E. Tomaszewski, J.L. Holleran, M. Muzzio, J. Eiseman, J.H. Beumer, J.H. Doroshow, Y. Pommier, NCI comparative oncology Program testing of non-camptothecin indenoisoquinoline topoisomerase I inhibitors in naturally occurring canine lymphoma, Clin. Cancer Res. 24 (2018) 5830–5840.
[20] X.J. Qin, Q. Yu, H. Yan, A. Khan, M.Y. Feng, P.P. Li, X.J. Hao, L.K. An, H.Y. Liu, Meroterpenoids with antitumor activities from guava (Psidium guajava), J. Agric. Food Chem. 65 (2017) 4993–4999.
[21] X.J. Qin, L.Y. Jin, Q. Yu, H. Liu, A. Khan, H. Yan, X.J. Hao, L.K. An, H.Y. Liu, A.-J. Eucalypglobulusals, Formyl-phloroglucinol-terpene meroterpenoids from Eucalyptus globulus fruits, J. Nat. Prod. 81 (2018) 2638–2646.
[22] X.R. Zhang, H.W. Wang, W.L. Tang, Y. Zhang, H. Yang, D.X. Hu, A. Ravji, C. Marchand, E. Kiselev, K. Ofori-Atta, K. Agama, Y. Pommier, L.K. An, Discovery, synthesis, and evaluation of oxynitidine derivatives as dual inhibitors of DNA topoisomerase IB (TOP1) and tyrosyl-DNA phosphodiesterase 1 (TDP1), and potential antitumor agents, J. Med. Chem. 61 (2018) 9908–9930.
[23] C.-C. Liu, R.P. Korivi, C.-H. Cheng, Cobalt-catalyzed regioselective synthesis of indenamine from o-iodobenzaldimine and alkyne: intriguing difference to the nickel-catalyzed reaction, Chem. Eur J. 14 (2008) 9503–9506.
[24] R.P. Korivi, C.H. Cheng, Protecting-group-free total synthesis of isoquinoline alkaloids by nickel-catalyzed annulation of o-halobenzaldimine with an alkyne as the key step, Chem. Eur J. 16 (2010) 282–287.
[25] M. Cushman, M. Jayaraman, J.A. Vroman, A.K. Fukunaga, B.M. Fox, G. Kohlhagen, D. Strumberg, Y. Pommier, Synthesis of new indeno[1,2-c]isoquinolines: cytotoxic non-camptothecin topoisomerase I inhibitors, J. Med. Chem. 43 (2000) 3688–3698.
[26] T.S. Dexheimer, Y. Pommier, DNA cleavage assay for the identification of topoisomerase I inhibitors, Nat. Protoc. 3 (2008) 1736–1750.
[27] Y. Urasaki, G.S. Laco, P. Pourquier, Y. Takebayashi, G. Kohlhagen, C. Gioffre, H. Zhang, D. Chatterjee, P. Pantazis, Y. Pommier, Characterization of a novel topoisomerase I mutation from a camptothecin resistant human prostate cancer cell line, Cancer Res. 61 (2001) 1964–1969.
[28] R.H. Shoemaker, The NCI60 human tumour cell line anticancer drug screen, Nat. Rev. Canc. 6 (2006) 813–823.
[29] S.L. Holbeck, J.M. Collins, J.H. Doroshow, Analysis of Food and Drug Administration-approved anticancer agents in the NCI60 panel of human tumor cell lines, Mol. Cancer Ther. 9 (2010) 1451–1460.
[30] W.C. Reinhold, M. Sunshine, S. Varma, J.H. Doroshow, Y. Pommier, Using cellMiner 1.6 for systems pharmacology and genomic analysis of the NCI-60, Clin. Cancer Res. 21 (2015) 3841–3852.
[31] Z.H. Miao, A. Player, U. Shankavaram, Y.H. Wang, D.B. Zimonjic, P.L. Lorenzi, Z.Y. Liao, H. Liu, T. Shimura, H.L. Zhang, L.H. Meng, Y.W. Zhang, E.S. Kawasaki, N.C. Popescu, M.I. Aladjem, D.J. Goldstein, J.N. Weinstein, Y. Pommier, Non-classic functions of human topoisomerase I: genome-wide and pharmacologic analyses, Cancer Res. 67 (2007) 8752–8761.
[32] Y.-H. Hsiang, R. Hertzberg, S. Hecht, L. Liu, Camptothecin induces protein-linked DNA breaks via mammalian DNA topoisomerase I, J. Biol. Chem. 260 (1985) 14873–14878.
[33] C.P. Wu, C.H. Hsieh, Y.S. Wu, The emergence of drug transporter-mediated multidrug resistance to cancer chemotherapy, Mol. Pharm. 8 (2011) 1996–2011.
[34] J. Zhu, R. Wang, L. Lou, W. Li, G. Tang, X. Bu, S. Yin, Jatrophane diterpenoids as modulators of P-Glycoprotein-Dependent multidrug resistance (MDR): advances of structure-activity relationships and discovery of promising MDR reversal agents, J. Med. Chem. 59 (2016) 6353–6369.
[35] J. Carmichael, W.G. DeGraff, A.F. Gazdar, J.D. Minna, J.B. Mitchell, Evaluation of a tetrazolium-based semiautomated colorimetrie assay: assessment of chemosensitivity testing, Cancer Res. 47 (1987) 936–942.
[36] J.C. Yalowich, X. Wu, R. Zhang, R. Kanagasabai, M. Hornbaker, B.B. Hasinoff, The anticancer thiosemicarbazones Dp44mT and triapine lack inhibitory effects as catalytic inhibitors or poisons of DNA topoisomerase IIalpha, Biochem. Pharmacol. 84 (2012) 52–58.
[37] D. Sooryakumar, T.S. Dexheimer, B.A. Teicher, Y. Pommier, Molecular and cellular pharmacology of the novel noncamptothecin topoisomerase I inhibitor Genz-644282, Mol. Cancer Ther. 10 (2011) 1490–1499.